Human Molecular Genetics, 2016, Vol. 25, No. 7 1357–1369

doi: 10.1093/hmg/ddw018
Advance Access Publication Date: 24 January 2016
Original Article

ORIGINAL ARTICLE

Collagen VI deficiency reduces muscle pathology, but does not improve muscle function, in the γ-sarcoglycan-null mouse

Jessica C. de Greef[1,2,3,4,†], Rebecca Hamlyn[1,2,3,4], Braden S. Jensen[1,2,3,4], Raul O'Campo Landa[1,2,3,4], Jennifer R. Levy[1,2,3,4], Kazuhiro Kobuke[1,2,3,4,‡] and Kevin P. Campbell[1,2,3,4,*]

[1]Howard Hughes Medical Institute, [2]Department of Molecular Physiology and Biophysics, [3]Department of Neurology and [4]Department of Internal Medicine, The University of Iowa Roy J. and Lucille A. Carver College of Medicine, Iowa City, IA 52242, USA

*To whom correspondence should be addressed at: Howard Hughes Medical Institute, The University of Iowa Roy J. and Lucille A. Carver College of Medicine, 4283 CBRB, 285 Newton Road, Iowa City, IA 52242, USA. Tel: +1 3193357867; Fax: +1 3193356957; Email: kevin-campbell@uiowa.edu

Abstract

Muscular dystrophy is characterized by progressive skeletal muscle weakness and dystrophic muscle exhibits degeneration and regeneration of muscle cells, inflammation and fibrosis. Skeletal muscle fibrosis is an excessive deposition of components of the extracellular matrix including an accumulation of Collagen VI. We hypothesized that a reduction of Collagen VI in a muscular dystrophy model that presents with fibrosis would result in reduced muscle pathology and improved muscle function. To test this hypothesis, we crossed γ-sarcoglycan-null mice, a model of limb-girdle muscular dystrophy type 2C, with a Col6a2-deficient mouse model. We found that the resulting γ-sarcoglycan-null/Col6a2Δex5 mice indeed exhibit reduced muscle pathology compared with γ-sarcoglycan-null mice. Specifically, fewer muscle fibers are degenerating, fiber size varies less, Evans blue dye uptake is reduced and serum creatine kinase levels are lower. Surprisingly, in spite of this reduction in muscle pathology, muscle function is not significantly improved. In fact, grip strength and maximum isometric tetanic force are even lower in γ-sarcoglycan-null/Col6a2Δex5 mice than in γ-sarcoglycan-null mice. In conclusion, our results reveal that Collagen VI-mediated fibrosis contributes to skeletal muscle pathology in γ-sarcoglycan-null mice. Importantly, however, our data also demonstrate that a reduction in skeletal muscle pathology does not necessarily lead to an improvement of skeletal muscle function, and this should be considered in future translational studies.

Introduction

Limb-girdle muscular dystrophy type 2C (LGMD2C) manifests clinically as a progressive muscle weakness with calf hypertrophy, elevated serum creatine kinase (CK) levels and onset occurs during childhood (1). This form of muscular dystrophy is caused by autosomal recessive mutations in the γ-sarcoglycan gene (SGCG; OMIM #253700), which encodes the transmembrane protein γ-sarcoglycan (γ-SG) (2). Together with α-SG, β-SG, δ-SG and sarcospan, γ-SG forms the SG complex in cardiac and skeletal

[†]Present address: Department of Human Genetics, Leiden University Medical Center, Leiden, the Netherlands.
[‡]Present address: Division of Cardiology, Department of Medicine, Kinki University Faculty of Medicine, Osaka, Japan.
Received: October 12, 2015. **Revised:** December 24, 2015. **Accepted:** January 18, 2016

muscle. This assembly of proteins contributes to stability of the sarcolemmal membrane in striated muscle and is part of the dystrophin–glycoprotein complex (DGC) (3). The DGC is present on the plasma membrane of muscle cells, where it links dystroglycan ligands within the extracellular matrix (ECM) to the cytoskeleton, thereby protecting muscle cells from contraction-induced injury (4). Deficiency of the SG proteins results in perturbation of the SG complex and in the development of a progressive muscular dystrophy (2,5–7). Muscle biopsies from patients with LGMD2C show signs of muscle fiber degeneration and regeneration (e.g. a high percentage of fibers with central nuclei and extensive variation in muscle fiber size), and increased endomysial and perimysial fibrosis.

Several mouse models lacking functional γ-SG have been generated (8,9). One is characterized by profoundly dystrophic muscles, the development of membrane disruptions in young mice, and premature death at ~20 weeks of age due to cardiomyopathy (8). A second γ-SG-null mouse model in which the same exon was targeted presents with similar phenotypic features related to skeletal and heart muscle degeneration, dystrophic changes in muscle, and interstitial fibrosis, yet these mice survive to over 1 year of age and exhibit progressive muscle hypertrophy starting at 12 weeks of age (9). The reasons for the differences in phenotype between these models remain unclear.

Fibrosis, an excessive accumulation of collagens and other ECM components, is a hallmark of many muscular dystrophies, including LGMD2C. One of the proteins deposited in the skeletal muscle ECM during fibrosis is Collagen VI (10). This is a microfibrillar protein that is present in many ECMs, including that of skeletal muscle, where it is concentrated in and adjacent to the basement membrane and contributes to maintaining the integrity of skeletal muscle. Collagen VI is composed of three distinct α-chains encoded by separate genes, *COL6A1*, *COL6A2* and *COL6A3*. Mutations in all three, both dominant and recessive, are associated with hereditary muscle disorders termed the Collagen VI-related myopathies, including Bethlem myopathy (11), Ullrich congenital muscular dystrophy (12) and myosclerosis myopathy (13). The clinical phenotypes of patients with Collagen VI-related myopathies are highly variable. For example, patients with Bethlem myopathy present with mild weakness of the proximal muscles and flexion contractures of the long fingers, elbows and ankles (14). Ullrich congenital muscular dystrophy is a more severe phenotype characterized by, next to muscle weakness and wasting, proximal joint contractures, distal hyperlaxity and normal intelligence (15).

Currently, the exact function of Collagen VI is still unknown. Collagen VI closely associates with the basement membrane around muscle cells and interacts *in vitro* with Collagen IV (16) and perlecan (17). Thus, it has been hypothesized that Collagen VI acts as an anchor for attachment of the basement membrane to the surrounding ECM and as such Collagen VI maintains basement membrane functional integrity. In line with this, muscle biopsies of patients with a mutation in one of the Collagen VI genes show basement membrane abnormalities, including unevenness, extension and folding, and overproduction of the basal lamina (18). Secondly, Collagen VI seems to be involved in tissue remodeling (19), wound healing (20), fibrosis (10) and muscle cell adhesion through its interactions with integrins (21) and the proteoglycan NG2 (22). Interestingly, when cultured *in vitro*, myogenic cells (both proliferating myoblasts and differentiating myotubes) are unable to deposit Collagen VI. Instead, Collagen VI is produced by the resident interstitial muscle fibroblasts (23).

Several mouse models have been generated for study of the Collagen VI-related myopathies. The first of these, which was described over 15 years ago, is a Col6a1-deficient mouse that produces no α1(VI) mRNA and in which Collagen VI protein is not deposited in the ECM. Muscles of both heterozygous and homozygous mice feature fiber necrosis and phagocytosis, pronounced variation in fiber size, and an increased percentage of centrally nucleated fibers. However, aside from these histopathological changes, no obvious phenotype is detected, and as such the mouse model is regarded a good representation of the mild Bethlem myopathy (24). Many years later, two additional Collagen VI mouse models were generated, both targeting the Col6a3 gene. One of these (the Col6a3$^{hm/hm}$ mouse) expresses a very low level of a non-functional α3(VI) mRNA, which results in the absence of Collagen VI from the ECM. Again, the myopathic pathology of these mice is limited (25). The second Col6a3 mouse model lacks Exon 16 of the Col6a3 gene (Col6a3$^{+/d16}$), mimicking the most common autosomal dominant mutation in Ullrich congenital muscular dystrophy patients. Mice heterozygous for this allele produce similar levels of the normal Col6a3 mRNA and an mRNA transcript with an in-frame deletion of 54 bp. The mutant α3(VI) protein exerts a dominant-negative effect on assembly of Collagen VI chains. The myopathic phenotype of these Col6a3$^{+/d16}$ mice, and of Col6a3$^{d16/d16}$ mice is again mild (26).

To study the consequences of Collagen VI deposition in the ECM of skeletal muscle during the development of muscular dystrophy, we crossed a γ-SG-null mouse model with a mouse model carrying an in-frame deletion of Exon 5 of the Col6a2 gene (Col6a2Δex5 mice). Both mouse models were recently generated in our lab. We hypothesized that Collagen VI ablation in a muscular dystrophy mouse model that features a significant amount of fibrosis would ameliorate the muscle pathology, thereby restoring some muscle function. We found that the γ-SG-null/Col6a2Δex5 mice indeed exhibited reduced muscle pathology, including reductions in the number of regenerating muscle fibers, variation in fiber size, Evans blue dye (EBD) uptake by skeletal muscles, and serum CK levels. However, muscle function was not improved, as assessed by measurements of grip strength and maximum isometric tetanic force.

Results

γ-SG-null mice exhibit severe muscle pathology including fibrosis

To study the pathogenesis of LGMD2C and to further unravel the function of γ-SG, we developed a γ-SG-null mouse model in our laboratory. We generated this mouse model using a targeting vector that contains Exon 2 followed by a fragment of Intron 2, and then a neomycin resistance cassette flanked by two loxP sites (Supplementary Material, Fig. S1A). Loss of γ-SG was confirmed by immunofluorescence staining, as well as the absence of α-SG, β-SG and δ-SG from the sarcolemma. Hematoxylin and eosin (H&E) staining showed that our γ-SG-null mice have severe muscle pathology similar to that commonly observed in patients with muscular dystrophy. It is characterized by a high percentage of centrally nucleated fibers and fiber size variation (Fig. 1A). In addition, high levels of serum CK levels were measured, both at baseline (Fig. 1B; $P < 0.001$) and 2 h after the mice completed a downhill exercise regime (Fig. 1B; $P < 0.05$). These features are indicative of a disruption of membrane integrity, a defect often observed in dystrophic muscles, although in our model this disruption did not seem to worsen after exercise.

As fibrosis is a hallmark of many muscular dystrophies, we also studied the muscles of our γ-SG-null mice by staining with Sirius red, a dye that binds to the $[Gly\text{-}X\text{-}Y]_n$ helix of fibrillar

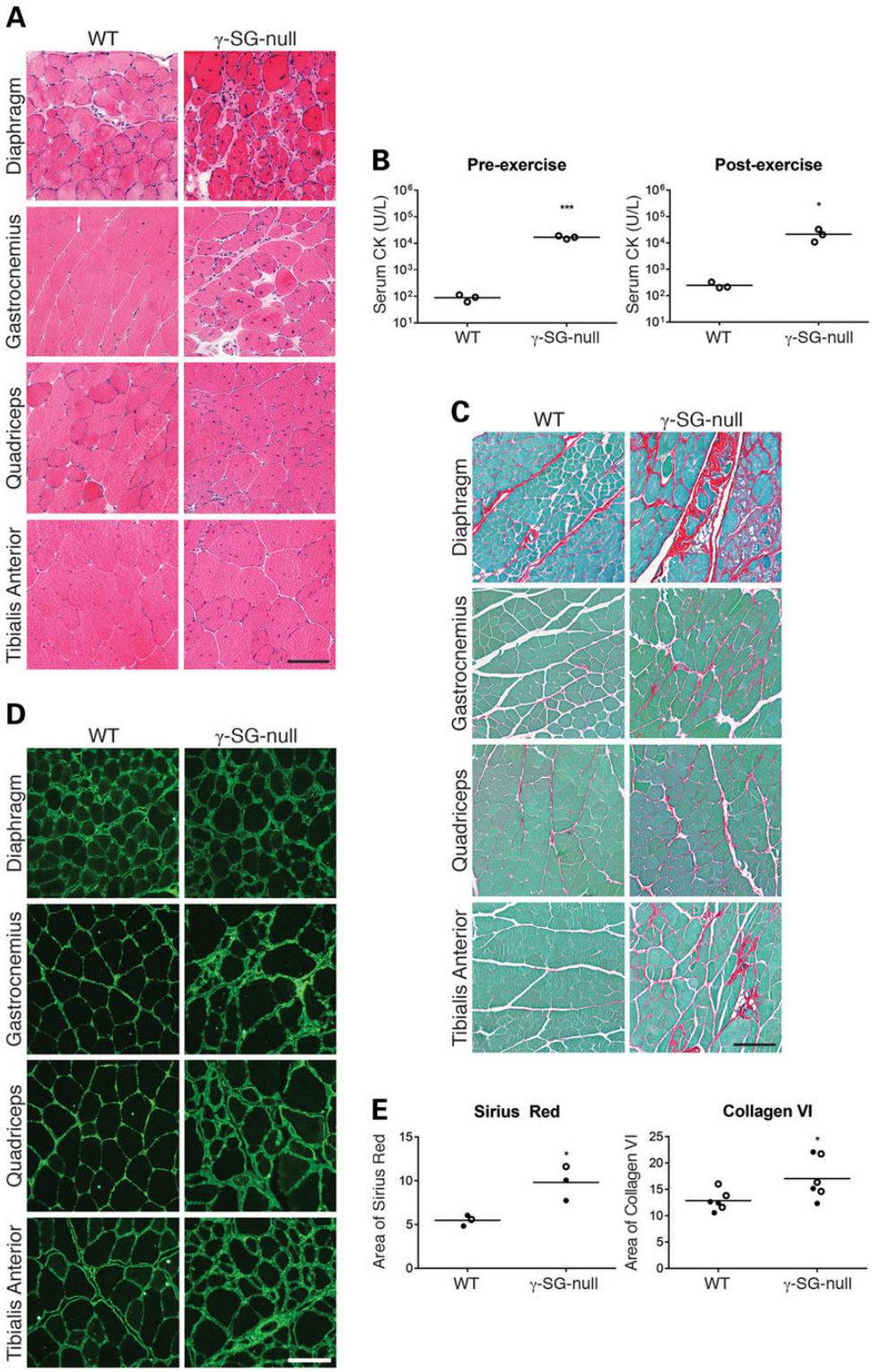

Figure 1. γ-SG-null mice exhibit severe muscle pathology including fibrosis. (**A**) Representative micrographs of H&E-stained muscles from WT and γ-SG-null mice (20–30 weeks of age). (**B**) Serum CK levels in WT and γ-SG-null mice (20 weeks of age) at baseline (pre-exercise) and 2 h after being subjected to a downhill exercise regime (post-exercise). $^{*}P < 0.05$ and $^{***}P < 0.001$. (**C**) Representative micrographs of Sirius red-stained muscles from WT and γ-SG-null mice (20–30 weeks of age). (**D**) Representative micrographs of Collagen VI-stained muscles from WT and γ-SG-null mice (20–30 weeks of age). (**E**) Quantification of Sirius red-stained and Collagen VI-stained quadriceps muscles from WT and γ-SG-null mice (20–30 weeks of age). $^{*}P < 0.05$. Samples shown in (A, C and D) were prepared and processed simultaneously, and images were taken at the same exposure level. Scale bar: 100 μm. Closed circles represent male mice, and open circles represent female mice in (B and E).

collagens, and mainly detects collagens I and III. We observed an increase in Sirius red staining in the ECM of all muscles examined in the γ-SG-null mice (Fig. 1C; quantification of Sirius red staining shown in Fig. 1E). We next performed immunofluorescence analysis of Collagen VI. In the γ-SG-null mice we detected Collagen VI deposition in the ECM of several muscles; in wild-type (WT) mice this deposition was restricted to the basement membrane (Fig. 1D; quantification of Collagen VI staining in Fig. 1E). Finally, we used immunofluorescence to examine the deposition of periostin, a non-collagen ECM component, in the γ-SG-null mice. Periostin, normally expressed in low amounts in muscle, is an adhesive molecule within the ECM and is activated by transforming growth factor-β (TGF-β). It can directly interact with Collagen I, and has been proposed to regulate Collagen I fibrillogenesis (27). Periostin levels were increased in our γ-SG-null mice (Supplementary Material, Fig. S2). Collectively these results show that the γ-SG-null mouse model we have generated presents with severe muscle pathology including an increase in deposition of fibrous connective tissue, consisting of at least collagens I and III (detected by Sirius red staining), Collagen VI and periostin.

Col6a2Δex5 mice present with a mild pathology

Previously described mouse models of Collagen VI-associated disease were generated by producing mutations in the Col6a1 and Col6a3 genes (24–26). As mutations in COL6A2 are also associated with disease, we generated a Col6a2 mouse model to test the contribution of this protein to the Collagen VI myopathies. Specifically, we used a targeting vector containing Exon 5 of Col6a2, and a neomycin resistance cassette flanked by two loxP sites (Supplementary Material, Fig. S1B). The Col6a2Δex5 mice carry an in-frame deletion of Exon 5, and mimic an autosomal dominant Col6a2 mutation found in a patient with Ullrich congenital muscular dystrophy (point mutation c.801G>A; does not result in an amino acid change, but skips Exon 5, as the affected nucleotide is part of the splice donor site). Homozygous mutants featured reduced Collagen VI staining in muscles, but heterozygotes appeared normal in this respect (Fig. 2A). This differs from the phenotype in the patient biopsy, where Collagen VI staining was reduced at specific locations of the basement membrane (data not shown). Moreover, we did not observe the mislocalization of Collagen VI with markers of the basement membrane that is typically seen in muscle biopsies of many patients with dominant-negative COL6 mutations. H&E staining of 12-week-old mice revealed limited muscle pathology in homozygous Col6a2Δex5 mice, including the presence of some centrally nucleated fibers (5–10%), variation in fiber size, and endomysial fibrosis (Fig. 2B). In mice over 1 year of age, the muscle phenotype remained mild, but was variable; variability was apparent when different muscles of an individual mouse were compared, as well as when similar muscles were compared across multiple mice.

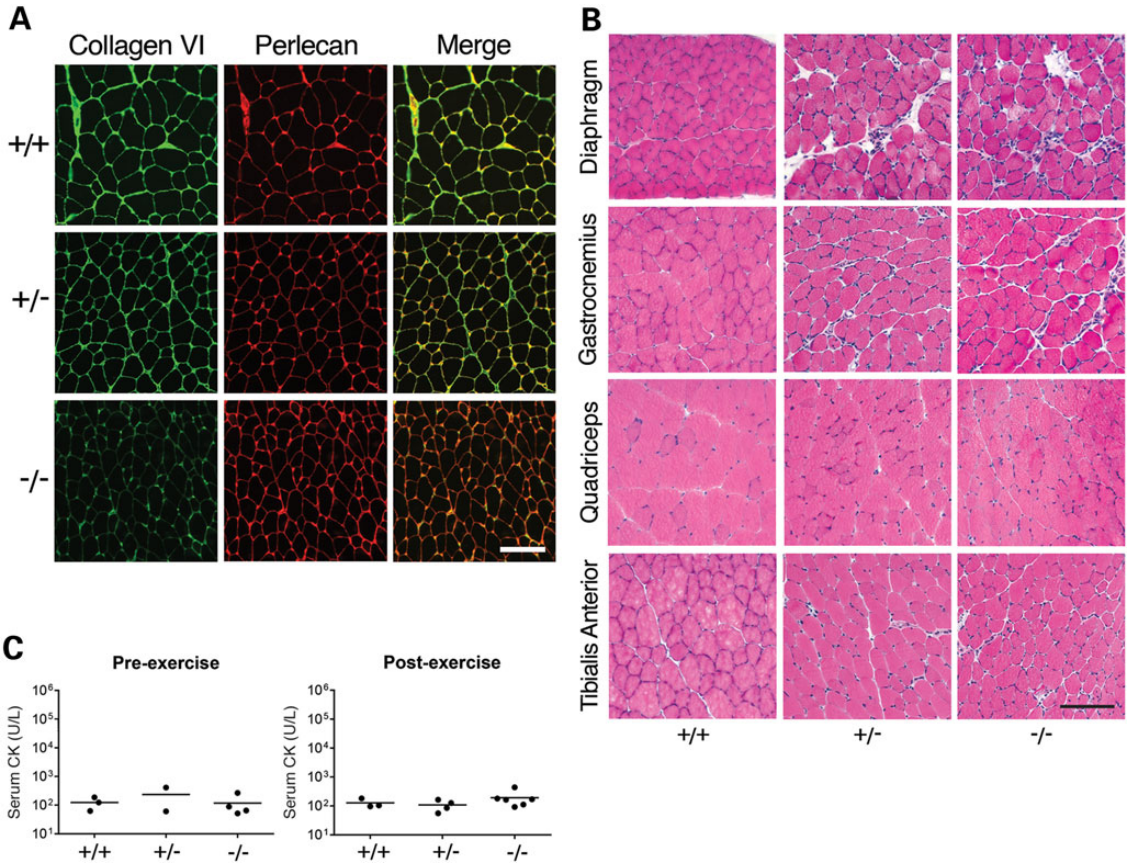

Figure 2. Col6a2Δex5 mice present with a mild pathology. (**A**) Representative micrographs of Collagen VI (green) and perlecan-stained (red) quadriceps muscles from WT (+/+), heterozygous (+/–) and homozygous (–/–) Col6a2Δex5 mice (12 weeks of age). (**B**) Representative micrographs of H&E-stained muscles from WT (+/+), heterozygous (+/–) and homozygous (–/–) Col6a2Δex5 mice (12 weeks of age). (**C**) Serum CK levels in WT (+/+), heterozygous (+/–) and homozygous (–/–) Col6a2Δex5 mice (50 weeks of age) at baseline (pre-exercise) and 2 h after downhill exercise (post-exercise). Closed circles represent male mice. Samples shown in (A and B) were prepared and processed simultaneously, and images were taken at the same exposure level. Scale bar: 100 μm.

Although only a small group of mice over 1 year of age has been tested thus far, the observed percentage of centrally nucleated fibers was 5–30% (data not shown). Finally, serum CK levels in mice carrying an Exon 5 deletion in Col6a2 were similar to those in WT littermates, both at baseline and 2 h after downhill exercise (Fig. 2C). Thus, homozygous Col6a2Δex5 mice present with a mild pathology, and deletion of Col6a2 Exon 5 does not seem to affect sarcolemmal integrity.

Decreased muscle pathology in γ-SG-null/Col6a2Δex5 mice

Our analysis of fibrous connective tissue in the γ-SG-null mouse model showed that one of the proteins that were increasingly deposited was Collagen VI (Fig. 1D and E). We observed a similar effect in the ECM of several other models of muscular dystrophy, including the *mdx* mouse model of Duchenne muscular dystrophy and the Large^{myd} mouse model of the dystroglycanopathies (data not shown). Although other studies have supported a role for Collagen VI during fibrosis (10), such a function has not been studied extensively in the context of muscular dystrophy progression. To elucidate the roles of Collagen VI during skeletal muscle fibrosis and in muscle pathology and muscle function, we crossed our Col6a2Δex5 mice with the γ-SG-null mice. In the offspring (WT; Col6a2Δex5 = Col6; γ-SG-null = γ-SG; γ-SG-null/Col6a2Δex5 = γ-SG/Col6), we first confirmed the presence or loss of γ-SG in muscle by western blotting, and that of Collagen VI staining in the basement membrane by immunofluorescence analysis (Supplementary Material, Fig. S3A and B). Next, we examined the extent of fibrosis using Sirius red staining. This revealed a decrease in Collagens I and III in the muscles of γ-SG/Col6 mice versus γ-SG mice (Fig. 3A; quantification of Sirius red staining of quadriceps muscles shown in Fig. 3G). Further, H&E staining (Fig. 3B) and perlecan/4′,6-diamidino-2-phenylindole (DAPI) immunofluorescence analysis (Supplementary Material, Fig. S3B) were performed to visualize and quantify the percentage of centrally nucleated fibers and variation in fiber size, respectively. Quantification of central nuclei and muscle fiber diameters suggest that the γ-SG/Col6 mice have milder muscle pathology compared with γ-SG mice; the number of regenerating muscle fibers was significantly reduced (Fig. 3C; $P < 0.0001$) and in three out of four muscles tested (diaphragm, quadriceps and tibialis anterior), fiber size varied (Fig. 3D; $P < 0.0001$). We also performed EBD uptake assays after a 30 min exercise regime (mice of all genotypes were able to finish this protocol), and observed less uptake by the skeletal muscles of γ-SG/Col6 mice versus γ-SG mice (Fig. 3E). These data are consistent with the serum CK levels we measured in these mice. Both at baseline and 2 h after exercise, serum CK levels were significantly lower in γ-SG/Col6 mice versus γ-SG mice (Fig. 3F; $P < 0.01$). In conclusion, the presence of a Col6a2Δex5 mutation in γ-SG-null mice prevented the muscle pathology otherwise observed in these animals.

Muscle function in γ-SG-null/Col6a2Δex5 mice is not improved

To determine the effect of a Col6a2 mutation on muscle function in γ-SG-null mice, we performed grip strength analysis and measured specific force production and force recovery following eight lengthening contractions (LCs) in the four different genotypes. Surprisingly, in spite of the observed rescue of pathology in the γ-SG/Col6 mice, grip strength (both two-limb and four-limb) was significantly lower in these animals than in their γ-SG littermates (Fig. 4A; $P < 0.0001$). This difference was not significantly affected by accounting for body weight (data not shown). As Col6 mice also presented with significantly reduced grip strength, we conclude that the presence of the Col6a2Δex5 mutation has a major impact on grip strength. To determine whether other SG-deficient mouse models also present with normal grip strength, we tested the α-SG-null and δ-SG-null mouse models, which are available in our laboratory (28, 29). At 8–10 weeks of age, both models show a significant reduction in four-limb grip strength (Supplementary Material, Fig. S4; $P < 0.0001$). It will be interesting to test all three SG-null mouse models at later time points to determine whether the muscle function in γ-SG-null mice decreases with age. Next, we examined specific force production in the extensor digitorum longus (EDL) muscle of these mice. This analysis revealed slight reduction in force production in γ-SG mice versus γ-SG/Col6 mice (Fig. 4B; $P < 0.05$). As specific force production by a muscle is dependent on muscle mass and fiber length, we also compared maximum isometric tetanic forces among the four genotypes and detected significantly lower tetanic force in γ-SG/Col6 mice versus γ-SG mice (Fig. 4C; $P < 0.0001$). Except in the case of the WT mice, all muscle from all of the mice exhibited a similar force deficit after eight LCs, as well as similar force recovery (Fig. 4D). These *ex vivo* tests suggest that both the Col6a2 mutation and loss of γ-SG impact muscle function. Thus, muscle function appears not to be improved in γ-SG-null mice with a homozygous Col6a2Δex5 mutation, regardless of whether tested *ex vivo* or *in vivo*.

γ-SG-null mice exhibit increases in both energy expenditure and lean mass

Skeletal muscle contributes significantly to whole-body energy metabolism as it is one of the most important tissues involved in whole body glucose uptake, especially when insulin levels are high. In addition, skeletal muscle is a major contributor of resting energy expenditure (EE) (30). Therefore, we decided to monitor the metabolic rate of our mice for 24 h using the comprehensive lab animal monitoring system (CLAMS). Oxygen consumption (VO_2), carbon dioxide production (VCO_2) and the respiratory exchange ratio (RER; the ratio between the amount of oxygen consumed and the amount of carbon dioxide produced, which indicates whether carbohydrate or fat is metabolized), did not differ across genotypes. Notably, EE was significantly higher in γ-SG mice than in γ-SG/Col6 mice (Fig. 5A; $P < 0.01$). This difference in EE could not be explained by differences in activity (Fig. 5B) or food intake (Supplementary Material, Fig. S5). As changes in EE may affect body composition, we next determined the body weight of the mice and performed nuclear magnetic resonance (NMR) analysis to measure differences in body composition among the four genotypes. Whereas γ-SG/Col6 mice had a lower body weight than γ-SG mice, a high-lean mass in the latter might account for this (Fig. 5C; $P < 0.0001$). Our results indicate that increased EE does not necessarily lead to reduced body weight. However, the fat mass of most γ-SG mice was lower than that of the γ-SG/Col6 mice. The higher body weight of γ-SG mice might be accounted for by muscle hypertrophy, as was observed in another γ-SG-null mouse model (9). Indeed, the combined weight of the gastrocnemius muscle, quadriceps muscle and tibialis anterior muscle was significantly higher in γ-SG mice than in γ-SG/Col6 mice (Fig. 5C; $P < 0.05$).

γ-SG-null mice that carry a heterozygous Col6a2Δex5 mutation have decreased muscle pathology, but not muscle function

Our Col6a2 mouse models an autosomal dominant patient mutation, yet in heterozygous form this mutation results in no or very

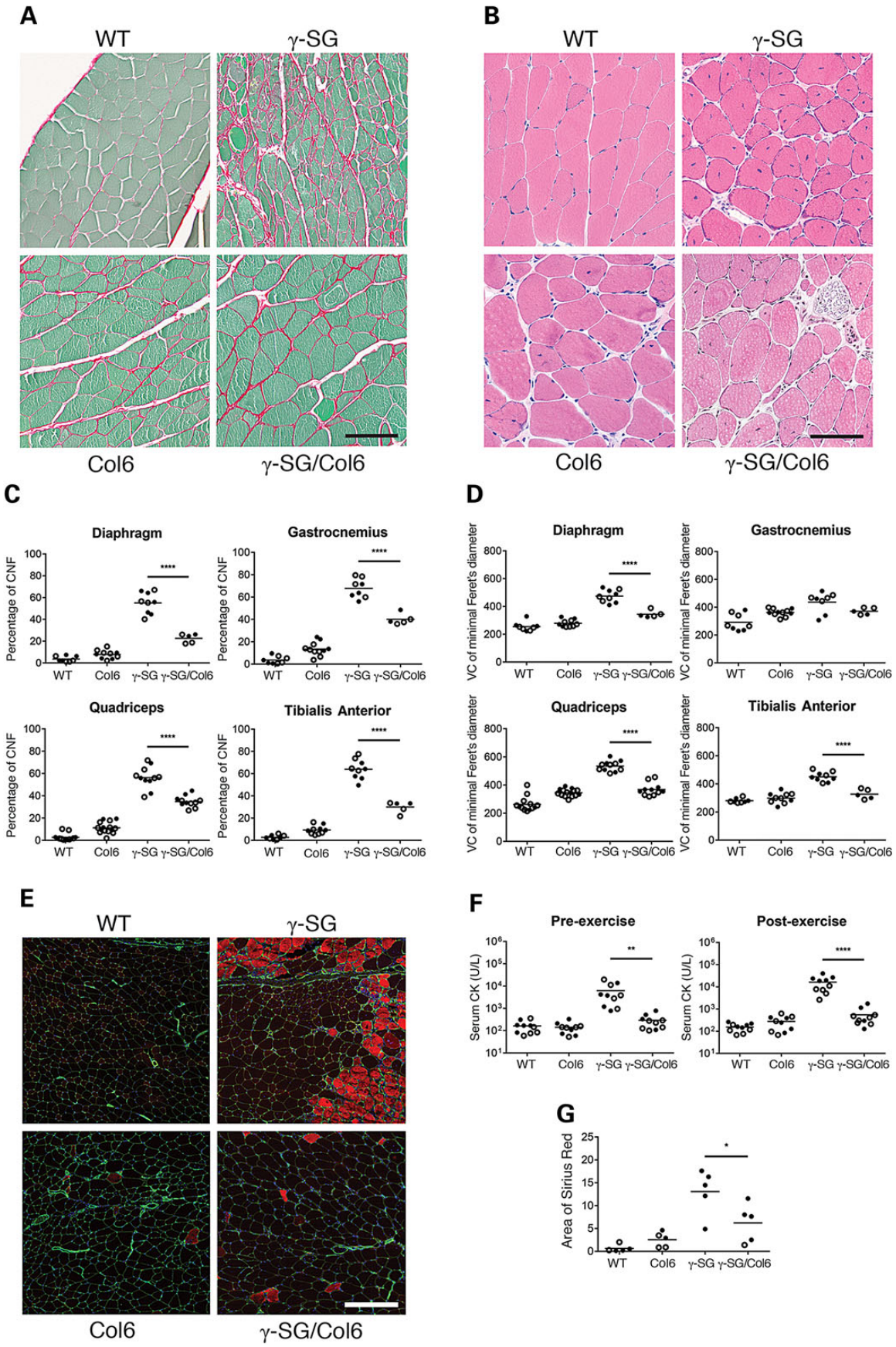
A
WT
γ-SG
Col6
γ-SG/Col6
B
WT
γ-SG
Col6
γ-SG/Col6
C
Diaphragm
Gastrocnemius
Quadriceps
Tibialis Anterior
Percentage of CNF
WT
Col6
γ-SG
γ-SG/Col6
****
D
Diaphragm
Gastrocnemius
Quadriceps
Tibialis Anterior
VC of minimal Feret's diameter
WT
Col6
γ-SG
γ-SG/Col6
****
E
WT
γ-SG
Col6
γ-SG/Col6
F
Pre-exercise
Post-exercise
Serum CK (U/L)
WT
Col6
γ-SG
γ-SG/Col6
**
****
G
Area of Sirius Red
WT
Col6
γ-SG
γ-SG/Col6
*

little muscle pathology. Given this mild phenotype, our studies thus far were carried out in homozygous mutant mice. However, considering the greatly reduced grip strength in the homozygous Col6a2Δex5 mice, we wondered whether the presence of a single Col6a2Δex5 allele would reduce the muscle pathology of the γ-SG-null mice without causing deterioration of muscle function. We, therefore, tested muscle pathology (percentage of centrally nucleated fibers and variation in fiber size), serum CK levels (at baseline and 2 h after downhill exercise) and grip strength (two-limb and four-limb-grip strength) in γ-SG-null mice heterozygous for the Col6a2Δex5 mutation. The results for muscle pathology and the serum CK levels looked promising, with the presence of a heterozygous Col6a2 mutation associated with reductions in the percentage of regenerating muscle fibers (Supplementary Material, Fig. S6A; $P < 0.0001$), variation in fiber size (Supplementary Material, Fig. S6B; $P < 0.0001$) and serum CK levels (Supplementary Material, Fig. S6C; $P < 0.01$), both pre- and post-exercise, relative to those in γ-SG-null mice. Nevertheless, grip strength was not significantly improved (Supplementary Material, Fig. S6D; $P < 0.0001$). Thus, although reduced deposition of Collagen VI in the ECM of γ-SG-null mice reduces muscle pathology, the effect of the Col6a2 mutation on muscle function is detrimental, regardless of whether heterozygous or homozygous.

Discussion

The main goal of the current study was to investigate whether a reduction of fibrosis, due to a Collagen VI deficiency, would reduce muscle pathology and improve muscle function in a mouse model of muscular dystrophy. Our initial analysis of a γ-SG-null mouse line and a Col6a2Δex5 mouse line showed that the phenotypes of these models are quite similar to those previously reported for other γ-SG-null (8,9) and Col6a1 and Col6a3 mutant (24–26) mouse models. However, with regard to longevity, our γ-SG-null mouse more closely resembles that generated by Sasaoka *et al.* (9) than that produced by Hack *et al.* (8), as these mice live well beyond 20 weeks of age. Despite the overt pathology, our γ-SG-null mice have grip strength comparable to that of WT mice. We believe that potential hypertrophy of the muscles of our γ-SG-null mice, as suggested by the increase in the weight of skeletal muscle, may explain the normal grip strength we observe. Consistent with this possibility, we observed only a small decrease in specific force production and an increase in maximum isometric tetanic force (in mice tested at 14–18 weeks of age). Although Hack *et al.* (31) reported no changes in force deficit in their γ-SG-null mouse model (13–16 weeks of age), this may be due to the use of a protocol involving fewer LCs and a lower percentage of lengthening.

Our Col6a2Δex5 mice present with a mild muscle phenotype. This is consistent with reports of other Collagen VI mouse models displaying a mild, sometimes progressive, muscle phenotype (24–26). Also, reduction in muscle contractile function was found in other Collagen VI mutant mouse models. However, whereas our Col6a2Δex5 mouse model presents with reduced grip strength and increased force deficit after eight LCs, neither Col6a3 mouse model showed a significant reduction in force after five eccentric contractions. Instead, the Col6a3$^{hm/hm}$ mice, which produce a non-functional Col6a3, presented with significantly reduced specific force production by the EDL muscle (25,26). Unfortunately, grip strength was not determined in these two mouse models. Again, the differences observed are most likely due to differences in the protocols employed to measure outcomes. Our discovery of increased EE in γ-SG-null mice is not surprising, given that similar results have been found in other muscular dystrophy mouse models, including the *mdx* mouse model of Duchenne muscular dystrophy (32). An increase in EE can most likely be explained by the impact of the disease process, which involves continuous cycles of degeneration and regeneration, on energy metabolism. Metabolic disorders such as obesity can affect the process of skeletal muscle repair (33), and it was recently shown that in mice with increased EE, a compensatory mechanism involving fiber-type switching, increased mitochondrial fission–fusion, and increased glucose metabolism had been activated (34). Thus, increased EE in the γ-SG-null mice may contribute to disease progression. Interestingly, EE in γ-SG-null/Col6a2Δex5 mice was comparable to that in WT and Col6a2Δex5 littermates. It is possible that the milder sarcolemmal disruption in γ-SG-null/Col6a2Δex5 mice versus γ-SG-null mice accounts for the reduction in muscle necrosis, regeneration and growth that occurs in these animals, and that the consequences for whole body energy metabolism are thus also more limited.

Our approach of reducing Collagen VI deposition in the skeletal muscle ECM through homozygous or heterozygous deficiency of Col6a2 could not improve the muscle function in γ-SG-null mice. Yet this study shows that Collagen VI-mediated fibrosis impacts skeletal muscle pathology, and the effect of this Collagen VI modulation on muscle pathology was greater than anticipated. The role of Collagen VI in skeletal muscle fibrosis in muscular dystrophy development will require further study. Notably, Collagen VI functions in the ECM of many other tissues than skeletal muscle, and we can obtain important clues regarding pathways and mechanisms involved from studies performed in these sites. For example, Collagen VI is the predominant collagen in the ECM of adipose tissue, where it provides mechanical support. However, in the diabetic state, Collagen VI and several other adipose tissue ECM components are up-regulated, resulting in mechanical stress on the adipocyte membrane. This can eventually result in necrosis, the recruitment of macrophages, and an inflammatory response. When Col6a1 was removed from this scenario, individual adipocytes expanded in uninhibited fashion, inflammation was reduced, and whole-body energy homeostasis was significantly improved (19). We have not yet investigated inflammation in the skeletal muscle of our mouse models, but will be interested to determine the effect of the Col6a2Δex5 mutation on the inflammatory response in the skeletal muscles of our γ-SG-null mice.

Figure 3. Muscle pathology is decreased in γ-SG-null/Col6a2Δex5 mice. (**A**) Representative micrographs of Sirius red-stained quadriceps muscles from WT, Col6, γ-SG and γ-SG/Col6 mice (14–20 weeks). (**B**) Representative micrographs of H&E-stained quadriceps muscles from WT, Col6, γ-SG and γ-SG/Col6 mice (14–18 weeks). (**C**) Quantification of the percentage of regenerating muscle fibers (CNFs, centrally nucleated fibers) in muscles from WT, Col6, γ-SG and γ-SG/Col6 mice (14–18 weeks). ****$P < 0.0001$. (**D**) Quantification of fiber size variation (VC = variance coefficient; 1000 × standard deviation of minimal Feret's diameter/mean of minimal Feret's diameter) in muscles from WT, Col6, γ-SG and γ-SG/Col6 mice (14–18 weeks). ****$P < 0.0001$. (**E**) Representative micrographs of EBD uptake (red) and perlecan (green) immunofluorescence staining in quadriceps muscles from WT, Col6, γ-SG and γ-SG/Col6 mice (12–16 weeks) after exercise. (**F**) Serum CK levels in WT, Col6, γ-SG and γ-SG/Col6 mice (10–12 weeks), both at baseline (pre-exercise) and 2 h after downhill exercise (post-exercise). **$P < 0.01$ and ****$P < 0.0001$. (**G**) Quantification of Sirius red-stained quadriceps muscles from WT, Col6, γ-SG and γ-SG/Col6 mice (14–20 weeks). *$P < 0.05$. Samples shown in (A, B and E) were prepared and processed simultaneously, and images were taken at the same exposure level. Scale bar: 100 μm (A and B) or 200 μm (**E**). Closed circles represent male mice, and open circles represent female mice in (C, D, F and G).

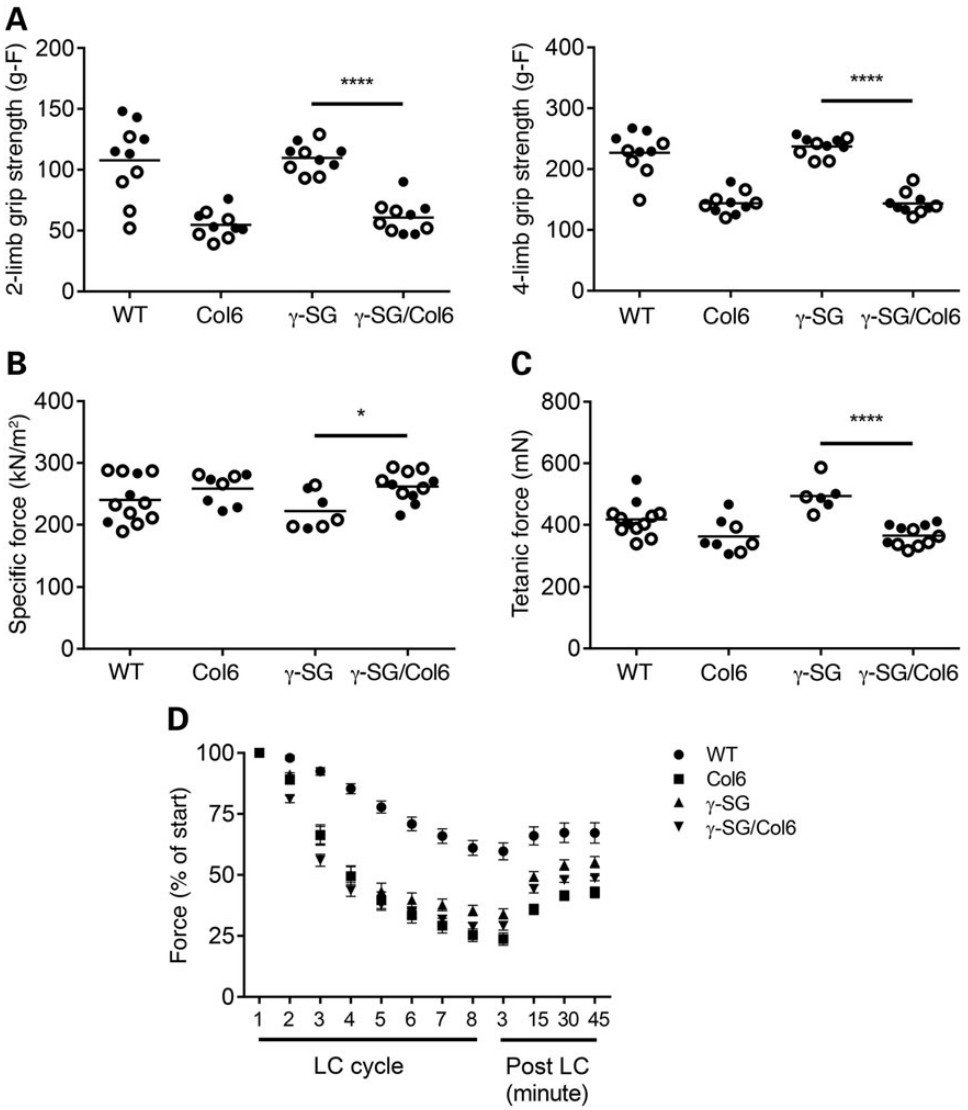

Figure 4. The muscle function in γ-SG-null/Col6a2Δex5 mice is not improved. (**A**) Two-limb and Four-limb grip strength in WT, Col6, γ-SG and γ-SG/Col6 mice (8–10 weeks). ****$P < 0.0001$. (**B**) Specific force production in WT, Col6, γ-SG and γ-SG/Col6 mice (14–18 weeks). *$P < 0.05$. (**C**) Maximum isometric tetanic force in WT, Col6, γ-SG and γ-SG/Col6 mice (14–18 weeks). *$P < 0.0001$. (**D**) Force deficit and force recovery following eight lengthening contractions in WT ($n = 8$), Col6 ($n = 7$), γ-SG ($n = 6$) and γ-SG/Col6 ($n = 9$) mice (14–18 weeks). Data are shown as mean ± standard error of the mean. Closed circles represent male mice, and open circles represent female mice in (A–C).

It may be prudent to test an alternative approach of Collagen VI modulation in γ-SG-null mice. Such an approach should not only prevent Collagen VI deposition in the skeletal muscle ECM as early as possible, preferably prior to any fibrotic tissue deposition, but also maintain correct association between Collagen VI and the basement membrane surrounding the muscle fibers. Possible approaches would be the inhibition of collagen synthesis and that of procollagen processing. Some agents affecting these processes have already been tested, mainly for Collagen type I. For example, the administration of analogues of proline, which constitutes ~10% of the amino acid content of collagens, has been shown to limit the accumulation of collagen in the lungs during pulmonary oxygen toxicity (35). Another possibility is the inhibition of bone morphogenetic protein-1 (BMP-1), the enzyme that cleaves C-terminal propeptides, and thus prevents fibril formation (36). Several uncertainties about such approaches exist, however. For example, whether the non-functional collagen molecules produced by these strategies will be deposited in the skeletal muscle ECM and affect muscle pathology and muscle function remains to be determined. In addition, some of these options are associated with significant toxicity (33). Should limitations with such approaches prove too great to be overcome, another option might involve taking advantage of the fact that Collagen VI is produced by interstitial muscle fibroblasts (23), i.e. targeting those. The disadvantage to such a strategy is that eliminating these cells could potentially affect other ECM components as well. The same disadvantage concerns BMP-1, which processes a number of non-collagen macromolecules (37,38) in addition to procollagens.

One of the most interesting findings of our study is that reducing muscle pathology (in this case by reducing Collagen VI levels and thereby reducing fibrosis), does not necessarily result in the normalized muscle function. γ-SG-null/Col6a2Δex5 mice present with lowgrip strength and maximum isometric tetanic force compared with γ-SG-null mice, in spite of the fact that muscle pathology (including serum CK levels and EBD uptake) was

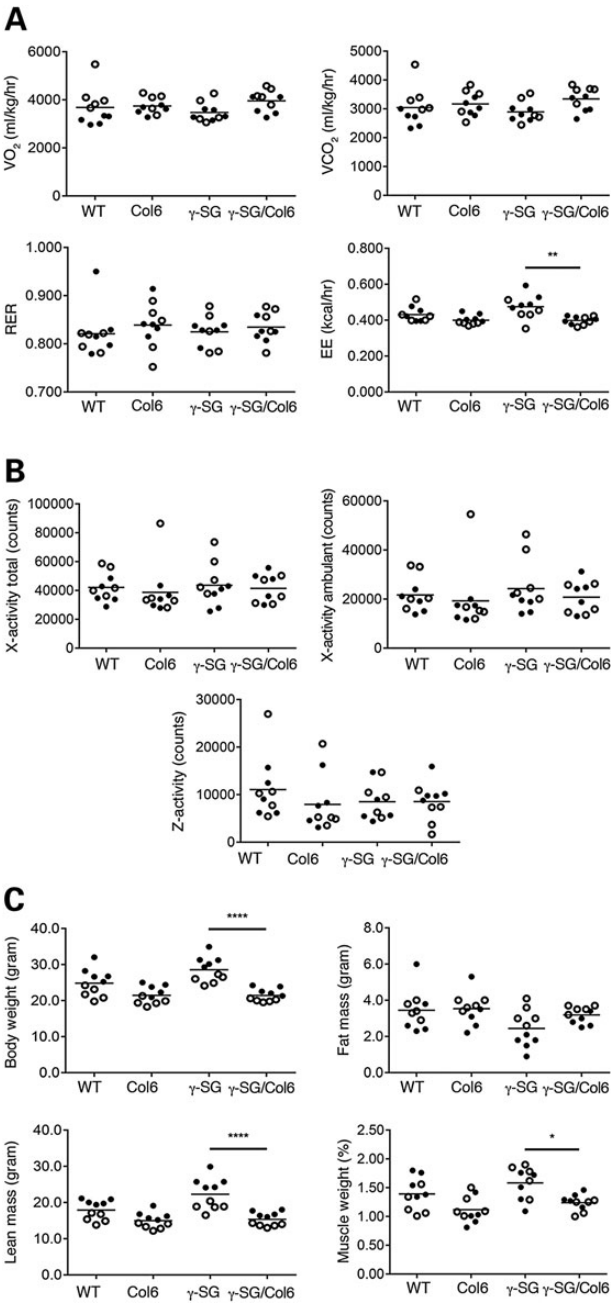

Figure 5. γ-SG-null mice exhibit increases in both EE and lean mass. (**A**) VO_2 VCO_2, RER and EE were recorded every 10 min in WT, Col6, γ-SG and γ-SG/Col6 mice (12–14 weeks) for 24 h. Average values for 24 h are shown. $^{**}P < 0.01$. (**B**) x-axis (total and ambulant) and z-axis activities of WT, Col6, γ-SG and γ-SG/Col6 mice (12–14 weeks) were recorded for 24 h. Total values for 24 h are shown. (**C**) The total body weight, fat mass and lean mass of WT, Col6, γ-SG and γ-SG/Col6 mice (12–14 weeks) was determined by NMR analysis. $^{****}P < 0.0001$. The combined weight, shown as the percentage of total body weight, of the gastrocnemius, quadriceps and tibialis anterior muscles from WT, Col6, γ-SG and γ-SG/Col6 mice (12–14 weeks) was determined after careful dissection. $^{*}P < 0.05$. Closed circles represent male mice, and open circles represent female mice in (A–C).

significantly reduced. Col6a2Δex5 mice, whose muscle pathology is even milder, also exhibited impaired grip strength and lower maximum isometric tetanic force. Our data suggest that muscle pathology and function are not directly related in the Collagen VI mouse model. In some studies, decreasing fibrosis seems sufficient to restore muscle function. For example, gene transfer of β-SG in the LGMD2E mouse model improved histological outcomes such as the percentage of centrally nucleated fibers, variation in fiber size and collagen deposition, and also restored tetanic force and force deficit (39). However, this approach was aimed at restoring the primary defect in LGMD2E. It will be interesting to test grip strength, specific force production and force deficit in δ-SG-null mice lacking the *Postn* gene, which encodes periostin. In these $Sgcd^{-/-}Postn^{-/-}$ mice, histopathology was improved and serum CK levels were lower than those in δ-SG-null mice. However, with regard to muscle function, only the time to fatigue by forced treadmill running was tested; no experiments testing muscle contractile function were performed (40). Since considerable basic research and some clinical trials currently focus on improving secondary defects associated with muscular dystrophy development, such as reduction of inflammation (41) or oxidative stress (42) and modulation of the TGF-β pathway, which plays an important role in the degeneration/regeneration response (43), it will be important to study both muscle pathology and function to determine whether a therapeutic agent ameliorates disease. Ultimately, combination treatments that target both simultaneously may offer the best therapeutic approach for many types of muscular dystrophy. For example, a recent study showed a promising outcome when gene replacement of micro-dystrophin was combined with delivery of the myostatin inhibitor follistatin for muscle enhancement (44).

In conclusion, this study shows that Collagen VI-mediated fibrosis contributes to skeletal muscle pathology in γ-SG-null mice. Notably, our data also reveal a disconnect between muscle pathology and muscle function, and this should be considered in future studies in both the basic research field and clinical trials.

Materials and Methods

Animals

WT littermates of the same genetic background and gender as the test animals were used as controls. In all studies, the experimenter was blinded to the genotypes of individual mice. Animal care, ethical usage and procedures were approved by the National Institutes of Health and the Animal Care Use and Review Committee at the University of Iowa, and were performed in strict accordance with these protocols. At the University of Iowa, all mice are housed socially (unless single housing is required), under specific pathogen-free conditions in an Association for Assessment and Accreditation of Laboratory Animal Care (AAALAC) accredited animal facility. Housing conditions are as specified in the Guide for the Care and Use of Laboratory Animals (National Research Council). Specifically, mice are housed on high-efficiency particulate air-filtered ventilated racks, in solid bottom cages (Thoren Caging Systems, Inc., Hazleton, PA, USA) with mixed paper bedding. A standard 12 h/12 h light/dark cycle is used. Standard rodent chow (Harlan Laboratories, Indianapolis, IN, USA) and water are available ad libitum.

Generation of γ-SG-null mice

Genomic fragments of the mouse γ-SG gene were obtained from bacterial artificial chromosome (BAC) clones isolated by polymerase chain reaction (PCR) screening of the CITB Mouse BAC DNA pool (#96021RG; Life Technologies, Carlsbad, CA, USA). A 4 kb fragment containing Exon 2 was used for the 5′-homologous arm, and a 2 kb fragment from Intron 2 was used for the 3′-homologous arm. These fragments were assembled with a phosphoglycerol kinase promoter-thymidine kinase cassette, a neomycin resistance cassette from a pcDNA3 plasmid (Agilent Technologies, Santa

Clara, CA, USA) flanked by two FLP (flippase) protein recombined sites, one loxP site 5′of Exon 2 and a second loxP site 3′ of the neomycin resistance cassette into a pBluescript IISK(–) plasmid (Agilent Technologies). The *Cla*I-linearized construct was electroporated into W4/129S6 ES cells (Taconic Biosciences, Hudson, NY, USA). Successful homozygous recombination at the 5′ and 3′ sides of the insertion was confirmed by PCR using the following primers: 5′-homologous recombination: F1, TAGCCGAAGAGAACAAAGCC AGAACAAACG and R1, GCAGCGCATCGCCTTCTATCGCCTTCTT; the 3′-homologous recombination: F2, GATCCTGCCCCGGCACTT CGCCCAATAG and R2, CCTCACCCCTGCCCTCCTGTCATGCCTTCC; the WT and the Exon 2-targeted alleles: F3, TTCTGCTCCCTTC CCCTCCCCGCTCTGA, R3–1, GCGAGATTCACAACGAGGATGGCGAG CAGGAGA, R3–2, TCGGGAAACCTTTTGGGCCTGGCATACT. In successfully recombined clones, the F1 and R1 and F2 and R2 primer pairs yielded bands of 8002 and 4151 bp, respectively. The F3 and R3–1 and F3 and R3–2 primer pairs produced bands of 326 bp from a WT locus, and of 376 bp from an Exon 2-targeted locus, respectively. The presence of coexisting random integrations of the targeting vector in recombinants was ruled out by Southern blot analysis, with a neomycin resistance cassette-encoding probe detecting only a single band on two independent restriction enzyme digests (*Bgl*II and *Eco*RI; data not shown). Correctly targeted ES cells were transfected with pCAGGS-FLPe to remove the neomycin resistance cassette. These γ-SG-floxed ES cells were further transfected with an EIIa Cre expression vector to remove the floxed Exon 2. The targeted clone was microinjected into C57BL/6J blastocysts, and chimeric mice were obtained. These mice were subsequently bred onto a C57BL/6J background for five generations. Genotyping of the γ-SG-null mice was carried out by PCR. The forward primer 5′-ATTCCCTCGAACCTTCTGCT-3′ and the reverse primer 5′-ATGTCCCATGATGCTCCAGT-3′ yield a 887 bp product from the WT allele and a 180 bp product from the γ-SG-null allele. Genotyping was confirmed by western blot analysis of skeletal muscle with a γ-SG antibody.

Generation of Col6a2Δex5 mice

Genomic fragments of the mouse Col6a2 gene were isolated from a 129-Sv genomic library. The Exon 5 coding region of Col6a2 was replaced by (i) a neomycin resistance cassette driven by the phosphoglycerol kinase promoter and flanked by FLP protein recombination sites and (ii) the Exon 5 coding region of Col6a2 flanked by loxP sites. The resulting targeting vector was linearized and electroporated into mouse 129/Sv embryonic stem cells. Neomycin resistant cell clones were screened by PCR, and positive clones were microinjected into C57BL/6J blastocysts. The resulting chimeric mice were crossed with C57BL/6J mice to obtain germline transmission of the homologous recombined Col6a2 allele. Next, Col6a2 mice were bred (i) with transgenic mice carrying a Cre recombinase gene driven by the adenovirus EIIa promoter (#003724; Jackson Laboratory, Bar Harbor, ME, USA) to delete Exon 5 of the Col6a2 gene and (ii) with transgenic mice carrying a flippase recombinase gene driven by the Gt (ROSA)26Sor promoter (#009086; Jackson Laboratory) to remove the neomycin resistance gene, resulting in the generation of Col6a2Δex5 mice. These mice were subsequently bred onto a C57BL/6J background for five generations. Genotyping of the Col6a2 Δex5 mice was carried out by PCR. The forward primer 5′-ATGCAAA AGGATGGAGGAAA-3′ and the reverse primer 5′-GCCCCATCA GAGTTCAGTGT-3′ yield a 1819 bp product from the WT allele and a 443 bp product from the Col6a2Δex5 allele. Genotyping was confirmed by immunofluorescence analysis of skeletal muscle co-stained with antibodies against Collagen VI and perlecan.

Antibodies

The following antibodies were obtained from the listed sources: anti-Collagen type VI (70R-CR009x; Fitzgerald Industries International, Acton, MA, USA); anti-heparan sulfate proteoglycan/perlecan clone A7L6 (RT-794; Thermo Fisher Scientific, Waltham, MA, USA); anti-periostin (ab92460; Abcam, Cambridge, MA, USA). The mouse monoclonal antibody against γ-SG (35DAG/21B5) was generated in collaboration with Louise V.B. Anderson (Newcastle General Hospital, Newcastle upon Tyne, UK).

Histological and immunofluorescence analysis

Mice were euthanized by cervical dislocation. Muscles (diaphragm, gastrocnemius, quadriceps and tibialis anterior) were dissected and frozen in isopentane cooled to –165°C in liquid nitrogen, or fixed overnight in 4% paraformaldehyde and embedded in paraffin by the Comparative Pathology Laboratory of the University of Iowa. For H&E staining, seven-micron cryosections were cut and fixed in 10% neutral buffered formalin (Thermo Fisher Scientific) for 5 min. After fixation, the slides were washed for 5 min under running water, followed by H&E staining consisting of several incubations with dH_2O, ethyl alcohol and xylene, a 1 min incubation in hematoxylin and a 20 s incubation in eosin. For Sirius red staining, five-micron paraffin sections were cut, followed by Sirius red staining consisting of several incubations with ethyl alcohol and xylene, and a 30 min incubation in 0.1% Sirius red F3B, C.O. 35730 (1A 280; Chroma Gesellschaft, Germany) in saturated picric acid (Sigma-Aldrich, St Louis, MO, USA) Both H&E- and Sirius red-stained sections were analyzed by light microscopy (Carl Zeiss Microscopy LLC, Thornwood, NY, USA). Immunofluorescence analysis was performed on seven-micron cryosections. Slides were blocked in 3% bovine serum albumin (BSA; Jackson ImmunoResearch, West Grove, PA) in phosphate-buffered saline (PBS) for 30 min, followed by overnight incubation in 1% BSA/PBS containing the antibody of interest. Sections were analyzed by fluorescence microscopy (Carl Zeiss Microscopy LLC) or using a VS120-S5-FL slide scanner microscope (Olympus, Center Valley, PA, USA) with the VS-ASW software (version 2.6.). The percentage of centrally nucleated muscle fibers and the fiber size diameter (minimal Feret's diameter) were determined on muscle sections co-stained with perlecan and DAPI (Sigma-Aldrich). Quantitative analysis was performed using the slide scanner microscope software (VSDEsktop software version 2.6.). For each individual mouse and each individual muscle, at least 500 fibers were analyzed, with the experimenter blinded to the genotypes of individual mice. For quantification of Sirius red staining, two regions of interest per tissues were saved as TIFFs tagged image file format and imported into ImageJ. Images were split into three channels (red, green and blue). The areas of the red and green regions were then calculated using ImageJ, and the relative fibrotic area was expressed as the ratio of red to green areas. For quantification of Collagen VI immunofluorescence staining, three regions of interest per tissue were saved as TIFFs and imported into ImageJ. Each was converted to an 8-bit image and thresholded using identical settings. The Analyze Particles function was used to measure the area of fluorescent signal.

Serum CK assay

Blood was collected by facial submandibular vein bleeds using Goldenrod 4 mm lancets (MEDIpoint, Inc., Mineola, NY, USA) and Microvette CB 300 tubes (Sarstedt Ag & Co, Newton, NC, USA). Blood was collected either before exercise or 2 h post-exercise, and the experimenter was blinded to the genotypes of

individual mice. For the downhill exercise regime, the mice were exercised with an adjustable variable-speed belt treadmill with a built-in shock grid from OmniPacer (Accuscan Instruments, Inc., Columbus, OH, USA). Mice were first acclimatized at a speed of 3 m/min for 5 min. Next, they were exercised at 15 m/min for 10 min, all at a 15° declination. Minimally 24 h were allowed between blood collections from the same mouse. Red blood cells were pelleted by centrifugation at 10 000*g* for 5 min, and serum was collected and analyzed immediately without freezing. Serum was diluted 1:49 (v:v) to ensure that activity levels were within the limits of the assay. Serum CK assays were performed in triplicate, using the CK Liqui-UV Test (Stanbio Laboratory, Boerne, TX, USA) according to the manufacturer's instructions. Absorbance at 340 nm was measured every 30 s for 2 min at 37°C, so that changes in enzyme activity could be calculated.

Western blot analysis

Skeletal muscle was homogenized using a Brinkmann Polytron Homogenizer (PT 10-35; Thermo Fisher Scientific), in 10 volumes of homogenization buffer (20 mM sodium phosphate monobasic, 20 mM sodium pyrophosphate, 0.303 M sucrose, 2 mM ethylenediaminetetraacetic acid, 1 mM $MgCl_2$, pH 7.1). Subsequently, samples were spun for 7 min at 10 000 rpm at 4°C (rotor JA20.1; Beckman Coulter, Brea, CA, USA) to remove non-homogenized material. Next, total microsomes were isolated from the supernatant by ultra-centrifugation for 22 min at 45 000 rpm at 4°C (rotor MLA-80; Beckman Coulter). The microsomes were washed twice with KCl wash buffer (50 mM Tris, 0.303 M sucrose, 0.6 M KCl, pH 7.4), with each wash step followed by another ultra-centrifugation step. Finally, KCl-washed microsomes were resuspended in 0.303 M sucrose, 20 mM Tris-maleate, at pH 7.0. All buffers contained the following protease inhibitors: pepstatin A (0.6 μg/ml), aprotinin (0.5 μg/ml), leupeptin (0.5 μg/ml), phenylmethylsulfonyl fluoride (0.1 mM), benzamidine (0.75 mM), calpain inhibitor I (2 μM) and calpeptin (2 μM). Protein samples were separated by 3–15% sodium dodecyl sulfate–polyacrylamide gel electrophoresis and transferred to polyvinylidene difluoride membranes (Immobilon FL-Membrane; Millipore, Billerica, MA, USA). The membranes were blocked in 5% milk in Tris-buffered saline containing 0.1% Tween-20 (TBS-T) and incubated with primary antibodies. Next, blots were washed with TBS-T and incubated with dye-conjugated secondary antibodies (Rockland Immunochemicals, Inc., Boyertown, PA, USA). After washing, blots were imaged using the Odyssey Imaging System (LI-COR, Lincoln, NE, USA).

EBD uptake

Fifty microliters of EBD solution, dissolved in PBS and sterilized by passage through a 0.2 μm membrane filter, were injected into the tail vein of the mice. The concentration of the injected dye was 0.5 mg EBD/0.05 ml PBS. Three hours after injection, the mice were exercised on an adjustable variable-speed belt treadmill with a built-in shock grid from OmniPacer (Accuscan Instruments, Inc.). Mice were first acclimatized at a speed of 3 meters/min for 5 min. Next, they were exercised at a 15° declination for (i) 5 min at 10 m/min, (ii) 5 min at 15 m/min, (iii) 5 min at 20 m/min and (iv) 10 min at 25 meters/min. All mice were able to finish this exercise protocol. Twenty-four hours later, the mice were euthanized by cervical dislocation, and the quadriceps muscles were dissected and frozen in isopentane cooled to −165°C in liquid nitrogen. Finally, seven-micron muscle sections were incubated in ice-cold acetone at −20°C for 10 min, washed in PBS three times for 10 min each and analyzed by fluorescence microscopy (Carl Zeiss Microscopy LLC).

Grip strength (two-limb and four-limb) analysis

For the two-limb (triangular trapeze bar) and four-limb (flat mesh pull bar) grip strength tests, mice were examined using a grip strength meter (Columbus Instruments, Columbus, OH, USA). The test was repeated five consecutive times within the same session, and the average of all trials was recorded. A minimum recovery period of 72 h was provided between the two-limb and four-limb tests. The experimenter was blinded to the genotypes of individual mice.

Force measurement

Contractile properties of EDL muscles were measured *ex vivo*. The mice were anesthetized with an intraperitoneal injection of 2% avertin (0.015 ml/g body weight), after which the EDL muscle was removed with tendons attached. The distal tendon was tied to a dual-mode servomotor (Aurora Scientific, Inc., Aurora, ON, Canada) using a 6-0 suture, and the proximal tendon was clamped to a fixed-force transducer (Aurora Scientific, Inc.). Next, the muscle was submerged in an oxygenated bath (95% O_2 and 5% CO_2) containing Ringer's solution (pH 7.4) at 25°C. Using twitches with pulse duration of 0.2 ms, the current of stimulation and the muscle length were increased to achieve the maximum isometric twitch force and optimal length (L_0), respectively. The fiber length (L_f) was then determined by multiplying L_0 by the ratio of the fiber length-to-muscle length. Next, while stimulating the EDL muscle for 300 ms, the stimulation frequency was increased until the force reached a plateau at maximum isometric tetanic force (P_0). Finally, the injury after eight LCs was assessed by subjecting the EDL muscle to one LC every 3 min. Each LC consisted of maximally activating the muscle at L_f, then stretching the muscle at a strain of 30% of L_f with a velocity of 1 L_f/s. The muscle was returned to L_0 at the same velocity. The force deficit was measured at 3, 15, 30 and 45 min after the eighth LCs. The total fiber cross-sectional area and specific force (kN/m^2) were calculated using muscle mass, L_f and P_0. The force deficit was defined as the difference between pre-LC force and post-LC force. Throughout the procedure, the experimenter was blinded to the genotypes of individual mice.

Metabolic cages

Mice were moved to the CLAMS (Columbus Instruments, Columbus, OH, USA) and acclimated for ~96 h. Next, food intake, indirect calorimetry (VO_2, VCO_2, RER (VCO_2/VO_2), EE [calorific value (CV) × VCO_2; CV = 3.815 + 1.232 × RER]) and *x*- and *z*-axis activity were measured over a 24 h period. The light/dark cycle and the temperature were constant before and during the experiment.

Nuclear magnetic resonance analysis

Fat mass and lean mass were assessed by time-domain-NMR. Non-sedated mice were placed into a vented plastic canister, which was next placed into the NMR machine (Bruker Minispec LD90, Bruker Optics, Inc., Billerica, MA, USA).

Statistical analysis

The data were compared using unpaired Student's *t*-test or analysis of variance followed by Holm–Sidak multiple-comparison tests when significance was detected ($P < 0.05$). Statistical analysis was performed using the SigmaPlot software (version 12.0.; Systat Software, Inc., Chicago, IL, USA), which determines if testing assumptions are met (Shapiro–Wilk normality and equal variance testing).

Supplementary Material

Supplementary Material is available at *HMG* online.

Acknowledgements

We thank Margaret Malik for providing experimental material for the BAC library screening. We also thank Keith Garringer and Erik Rader for technical assistance. We especially thank Christine Blaumueller for critical reading of the manuscript. We are grateful to past and current members of the Campbell Laboratory for insightful comments and fruitful discussions. We thank Baoli Yang and Renee Goodfellow (University of Iowa Gene Targeting Core Facility) for generating the Col6a2Δex5 mice.

Conflict of Interest statement. None declared.

Funding

This work was supported in part by National Institutes of Health grant T32HL007121 through National Heart, Lung, and Blood Institute (to J.R.L.), Muscular Dystrophy Association Development grant MDA200826 (to J.R.L.) and a Paul D. Wellstone Muscular Dystrophy Cooperative Research Center grant (1U54NS053672). K.P.C. is an investigator of the Howard Hughes Medical Institute. Funding to pay the Open Access publication charges for this article was provided by the Howard Hughes Medical Institute.

References

1. Kirschner, J. and Lochmüller, H. (2011) Sarcoglycanopathies. *Handb. Clin. Neurol.*, **101**, 41–46.
2. Noguchi, S., McNally, E.M., Ben Othmane, K., Hagiwara, Y., Mizuno, Y., Yoshida, M., Yamamoto, H., Bönnemann, C.G., Gussoni, E., Denton, P.H. *et al.* (1995) Mutations in the dystrophin-associated protein gamma-sarcoglycan in chromosome 13 muscular dystrophy. *Science*, **270**, 819–822.
3. Crosbie, R.H., Lebakken, C.S., Holt, K.H., Venzke, D.P., Straub, V., Lee, J.C., Grady, R.M., Chamberlain, J.S., Sanes, J.R. and Campbell, K.P. (1999) Membrane targeting and stabilization of sarcospan is mediated by the sarcoglycan subcomplex. *J. Cell. Biol.*, **145**, 153–165.
4. Matsumura, K. and Campbell, K.P. (1994) Dystrophin-glycoprotein complex: its role in the molecular pathogenesis of muscular dystrophies. *Muscle Nerve*, **17**, 2–15.
5. Roberds, S.L., Leturcq, F., Allamand, V., Piccolo, F., Jeanpierre, M., Anderson, R.D., Lim, L.E., Lee, J.C., Tomé, F.M.S., Romero, N.B. *et al.* (1994) Missense mutations in the adhalin gene linked to autosomal recessive muscular dystrophy. *Cell*, **78**, 625–633.
6. Bönnemann, C.G., Modi, R., Noguchi, S., Mizuno, Y., Yoshida, M., Gussoni, E., McNally, E.M., Duggan, D.J., Angelini, C. and Hoffman, E.P. (1995) Beta-sarcoglycan (A3b) mutations cause autosomal recessive muscular dystrophy with loss of the sarcoglycan complex. *Nat. Genet.*, **11**, 266–273.
7. Nigro, V., de Sá Moreira, E., Piluso, G., Vainzof, M., Belsito, A., Politano, L., Puca, A.A., Passos-Bueno, M.R. and Zatz, M. (1996) Autosomal recessive limb-girdle muscular dystrophy, LGMD2F, is caused by a mutation in the delta-sarcoglycan gene. *Nat. Genet.*, **14**, 195–198.
8. Hack, A.A., Ly, C.T., Jiang, F., Clendenin, C.J., Sigrist, K.S., Wollmann, R.L. and McNally, E.M. (1998) Gamma-sarcoglycan deficiency leads to muscle membrane defects and apoptosis independent of dystrophin. *J. Cell. Biol.*, **142**, 1279–1287.
9. Sasaoka, T., Imamura, M., Araishi, K., Noguchi, S., Mizuno, Y., Takagoshi, N., Hama, H., Wakabayashi-Takai, E., Yoshimoto-Matsuda, Y., Nonaka, I. *et al.* (2003) Pathological analysis of muscle hypertrophy and degeneration in muscular dystrophy in gamma-sarcoglycan-deficient mice. *Neuromuscul. Disord.*, **13**, 193–206.
10. Zanotti, S., Saredi, S., Ruggieri, A., Fabbri, M., Blasevich, F., Romaggi, S., Morandi, L. and Mora, M. (2007) Altered extracellular matrix transcript expression and protein modulation in primary Duchenne muscular dystrophy myotubes. *Matrix Biol.*, **26**, 615–624.
11. Jöbsis, G.J., Keizers, H., Vreijling, J.P., de Visser, M., Speer, M.C., Wolterman, R.A., Baas, F. and Bolhuis, P.A. (1996) Type VI collagen mutations in Bethlem myopathy, an autosomal dominant myopathy with contractures. *Nat. Genet.*, **14**, 113–115.
12. Camacho Vanegas, O., Bertini, E., Zhang, R.Z., Petrini, S., Minosse, C., Sabatelli, P., Giusti, B., Chu, M.L. and Pepe, G. (2001) Ullrich scleroatonic muscular dystrophy is caused by recessive mutations in collagen type VI. *Proc. Natl Acad. Sci. U S A*, **98**, 7516–7521.
13. Merlini, L., Martoni, E., Grumati, P., Sabatelli, P., Squarzoni, S., Urciuolo, A., Ferlini, A., Gualandi, F. and Bonaldo, P. (2008) Autosomal recessive myosclerosis myopathy is a collagen VI disorder. *Neurology*, **71**, 1245–1253.
14. Bethlem, J. and Wijngaarden, G.K. (1976) Benign myopathy, with autosomal dominant inheritance. A report on three pedigrees. *Brain*, **99**, 91–100.
15. Ullrich, O. (1930) Kongenitale atonisch-sklerotische Muskeldystrophie. *Monatsschr. Kinderheilkd.*, **47**, 502–510.
16. Kuo, H.J., Maslen, C.L., Keene, D.R. and Glanville, R.W. (1997) Type VI collagen anchors endothelial basement membranes by interacting with type IV collagen. *J. Biol. Chem.*, **272**, 26522–26529.
17. Tillet, E., Wiedemann, H., Golbik, R., Pan, T.C., Zhang, R.Z., Mann, K., Chu, M.L. and Timpl, R. (1994) Recombinant expression and structural and binding properties of alpha 1(VI) and alpha 2(VI) chains of human collagen type VI. *Eur. J. Biochem.*, **221**, 177–185.
18. Niiyama, T., Higuchi, I., Suehara, M., Hashiguchi, T., Shiraishi, T., Nakagawa, M., Arimura, K., Maruyama, I. and Osame, M. (2002) Electron microscopic abnormalities of skeletal muscle in patients with collagen VI deficiency in Ullrich's disease. *Acta. Neuropathol.*, **104**, 67–71.
19. Khan, T., Muise, E.S., Iyengar, P., Wang, Z.V., Chandalia, M., Abate, N., Zhang, B.B., Bonaldo, P., Chua, S. and Scherer, P.E. (2009) Metabolic dysregulation and adipose tissue fibrosis: role of collagen VI. *Mol. Cell. Biol.*, **29**, 1575–1591.
20. Oono, T., Specks, U., Eckes, B., Majewski, S., Hunzelmann, N., Timpl, R. and Krieg, T. (1993) Expression of type VI collagen mRNA during wound healing. *J. Invest. Dermatol.*, **100**, 329–334.
21. Pfaff, M., Aumailley, M., Specks, U., Knolle, J., Zerwes, H.G. and Timpl, R. (1993) Integrin and Arg-Gly-Asp dependence of cell adhesion to the native and unfolded triple helix of collagen type VI. *Exp. Cell. Res.*, **206**, 167–176.
22. Burg, M.A., Tillet, E., Timpl, R. and Stallcup, W.B. (1996) Binding of the NG2 proteoglycan to type VI collagen and other extracellular matrix molecules. *J. Biol. Chem.*, **271**, 26110–26116.
23. Zou, Y., Zhang, R.Z., Sabatelli, P., Chu, M.L. and Bönnemann, C.G. (2008) Muscle interstitial fibroblasts are the main source of collagen VI synthesis in skeletal muscle: implications for congenital muscular dystrophy types Ullrich and Bethlem. *J. Neuropathol. Exp. Neurol.*, **67**, 144–154.

24. Bonaldo, P., Braghetta, P., Zanetti, M., Piccolo, S., Volpin, D. and Bressan, G.M. (1998) Collagen VI deficiency induces early onset myopathy in the mouse: an animal model for Bethlem myopathy. *Hum. Mol. Genet.*, **7**, 2135–2140.
25. Pan, T.C., Zhang, R.Z., Markova, D., Arita, M., Zhang, Y., Bogdanovich, S., Khurana, T.S., Bönnemann, C.G., Birk, D.E. and Chu, M.L. (2013) COL6A3 protein deficiency in mice leads to muscle and tendon defects similar to human collagen VI congenital muscular dystrophy. *J. Biol. Chem.*, **288**, 14320–14331.
26. Pan, T.C., Zhang, R.Z., Arita, M., Bogdanovich, S., Adams, S.M., Gara, S.K., Wagener, R., Khurana, T.S., Birk, D.E. and Chu, M.L. (2014) A mouse model for dominant collagen VI disorders: heterozygous deletion of Col6a3 Exon 16. *J. Biol. Chem.*, **289**, 10293–102307.
27. Norris, R.A., Damon, B., Mironov, V., Kasyanov, V., Ramamurthi, A., Moreno-Rodriguez, R., Trusk, T., Potts, J.D., Goodwin, R.L., Davis, J. *et al.* (2007) Periostin regulates collagen fibrillogenesis and the biomechanical properties of connective tissues. *J. Cell. Biochem.*, **101**, 695–711.
28. Duclos, F., Straub, V., Moore, S.A., Venzke, D.P., Hrstka, R.F., Crosbie, R.H., Durbeej, M., Lebakken, C.S., Ettinger, A.J., van der Meulen, J. *et al.* (1998) Progressive muscular dystrophy in alpha-sarcoglycan-deficient mice. *J. Cell. Biol.*, **142**, 1461–1471.
29. Coral-Vazquez, R., Cohn, R.D., Moore, S.A., Hill, J.A., Weiss, R.M., Davisson, R.L., Straub, V., Barresi, R., Bansal, D., Hrstka, R.F. *et al.* (1999) Disruption of the sarcoglycan-sarcospan complex in vascular smooth muscle: a novel mechanism for cardiomyopathy and muscular dystrophy. *Cell*, **98**, 465–474.
30. Zurlo, F., Larson, K., Bogardus, C. and Ravussin, E. (1990) Skeletal muscle metabolism is a major determinant of resting energy expenditure. *J. Clin. Invest.*, **86**, 1423–1427.
31. Hack, A.A., Cordier, L., Shoturma, D.I., Lam, M.Y., Sweeney, H.L. and McNally, E.M. (1999) Muscle degeneration without mechanical injury in sarcoglycan deficiency. *Proc. Natl Acad. Sci. U S A*, **96**, 10723–10728.
32. Radley-Crabb, H.G., Marini, J.C., Sosa, H.A., Castillo, L.I., Grounds, M.D. and Fiorotto, M.L. (2014) Dystropathology increases energy expenditure and protein turnover in the mdx mouse model of Duchenne muscular dystrophy. *PLoS One*, **9**, e89277.
33. Akhmedov, D. and Berdeaux, R. (2013) The effects of obesity on skeletal muscle regeneration. *Front. Physiol.*, **4**, 371.
34. Pant, M., Sopariwala, D.H., Bal, N.C., Lowe, J., Delfín, D.A., Rafael-Fortney, J. and Periasamy, M. (2015) Metabolic dysfunction and altered mitochondrial dynamics in the utrophin-dystrophin deficient mouse model of Duchenne muscular dystrophy. *PLoS One*, **10**, e0123875.
35. Riley, D.J., Berg, R.A., Edelman, N.H. and Prockop, D.J. (1980) Prevention of collagen deposition following pulmonary oxygen toxicity in the rat by cis-4-hydroxy-L-proline. *J. Clin. Invest.*, **65**, 643–651.
36. Li, S.W., Sieron, A.L., Fertala, A., Hojima, Y., Arnold, W.V. and Prockop, D.J. (1996) The C-proteinase that processes procollagens to fibrillar collagens is identical to the protein previously identified as bone morphogenic protein-1. *Proc. Natl Acad. Sci. U S A*, **93**, 5127–5130.
37. Amano, S., Scott, I.C., Takahara, K., Koch, M., Champliaud, M.F., Gerecke, D.R., Keene, D.R., Hudson, D.L., Nishiyama, T., Lee, S. *et al.* (2000) Bone morphogenetic protein 1 is an extracellular processing enzyme of the laminin 5 gamma 2 chain. *J. Biol. Chem.*, **275**, 22728–22735.
38. Scott, I.C., Imamura, Y., Pappano, W.N., Troedel, J.M., Recklies, A.D., Roughley, P.J. and Greenspan, D.S. (2000) Bone morphogenetic protein-1 processes probiglycan. *J. Biol. Chem.*, **275**, 30504–30511.
39. Pozsgai, E.R., Griffin, D.A., Heller, K.N., Mendell, J.R. and Rodino-Klapac, L.R. (2016) β-Sarcoglycan gene transfer decreases fibrosis and restores force in LGMD2E mice. *Gene Ther.*, **23**, 57–66.
40. Lorts, A., Schwanekamp, J.A., Baudino, T.A., McNally, E.M. and Molkentin, J.D. (2012) Deletion of periostin reduces muscular dystrophy and fibrosis in mice by modulating the transforming growth factor-β pathway. *Proc. Natl Acad. Sci. U S A*, **109**, 10978–10983.
41. Zschüntzsch, J., Zhang, Y., Klinker, F., Makosch, G., Klinge, L., Malzahn, D., Brinkmeier, H., Liebetanz, D. and Schmidt, J. (2015) Treatment with human immunoglobulin G improves the early disease course in a mouse model of Duchenne muscular dystrophy. *J. Neurochem.*, Epub ahead of print.
42. Whitehead, N.P., Kim, M.J., Bible, K.L., Adams, M.E. and Froehner, S.C. (2015) A new therapeutic effect of simvastatin revealed by functional improvement in muscular dystrophy. *Proc. Natl Acad. Sci. U S A*, **112**, 12864–12869.
43. Accornero, F., Kanisicak, O., Tjondrokoesoemo, A., Attia, A.C., McNally, E.M. and Molkentin, J.D. (2014) Myofiber-specific inhibition of TGFβ signaling protects skeletal muscle from injury and dystrophic disease in mice. *Hum. Mol. Genet.*, **23**, 6903–6915.
44. Rodino-Klapac, L.R., Janssen, P.M., Shontz, K.M., Canan, B., Montgomery, C.L., Griffin, D., Heller, K., Schmelzer, L., Handy, C., Clark, K.R. *et al.* (2013) Micro-dystrophin and follistatin co-delivery restores muscle function in aged DMD model. *Hum. Mol. Genet.*, **22**, 4929–4937.